

Magnetic spin excitations in Mn doped GaAs : A model study

Akash Chakraborty¹, Richard Bouzerar¹ and Georges Bouzerar^{1,2}

1. Institut Néel, CNRS, Département MCBT, 25 avenue des Martyrs, B.P. 166, 38042 Grenoble Cedex 09, France

2. School of Engineering and Science, Jacobs University Bremen, Campus Ring 1, D-28759 Bremen, Germany

(Dated: October 14, 2019)

We provide a quantitative theoretical model study of the dynamical magnetic properties of optimally annealed $\text{Ga}_{1-x}\text{Mn}_x\text{As}$. Both the calculated Curie temperatures and spin stiffness are found to be in excellent agreement with those obtained from ab-initio studies. An overall good agreement is found between theory and experiments. We have also evaluated the magnon density of states and the “mobility edge” which separates extended from localized states. The power of the model lies in its ability to be generalized for a broad class of diluted magnetic semiconductor materials, thus it bridges the gap between first principle calculations and model studies.

PACS numbers: 75.50.Pp, 75.30.Ds, 71.55.Eq

The prospect of manipulating the electronic spin for spintronics applications has generated a tremendous interest in the so called diluted magnetic semiconductors (DMS) over the past few years[1, 2]. Among the whole family of III-V semiconductors, Mn doped GaAs is the most widely studied. The understanding of its fundamental physical properties involves large theoretical speculations[3–5]. Like it is well established that the ferromagnetic ordering is mediated by holes arising from Mn ions but there is still a controversy regarding the existence of a preformed impurity band (IB) in GaMnAs. Most of the model studies are based on a perturbative treatment of Mn in GaAs (the valence band (VB) picture)[2, 3]. This is in contradiction to the ab-initio calculations[9, 10], which shows that Mn strongly affects the nature of the states close to the Fermi level (E_F) which supports the IB picture. Experiments based on infrared and optical spectroscopy have shown that E_F resides indeed in a Mn induced IB in GaMnAs[11]. Now regarding the model approaches, the most frequently studied model is based on a six or eight band Kohn-Luttinger Hamiltonian[2, 3]. In this approach the p-d-coupling is treated perturbatively and the dilution effects are neglected (the VB picture), which as aforementioned are incompatible with the ab-initio based studies. Note that it has been demonstrated before that the perturbative treatment is inappropriate for DMS[12, 13]. Although the first principle calculations were able to reproduce the Curie temperatures accurately[6–8] they are essentially material specific. Hence the ideal tool to identify and analyze the effect of the relevant physical parameters is a minimal model approach based on a non-perturbative treatment of the substitution effects.

In this letter we use the one band V-J model[13], treated non-perturbatively, to study the dynamical magnetic properties of the III-V DMS GaMnAs, which will be shown to provide the missing link between ab-initio and model studies. To be more specific we adopt a two-step approach to calculate the magnetic properties of GaMnAs. To start with the couplings between the magnetic

impurities are calculated within the one band V-J model without the use of any effective medium theory. In the second step the effective dilute Heisenberg Hamiltonian is treated within the self consistent local RPA (SC-LRPA) theory to calculate the magnetic properties as well as the T_{CS} . It is to be noted that the accuracy and reliability of SC-LRPA to treat dilution/disorder and thermal fluctuations has been proved time and again[8, 14]. The non-perturbative treatment of the V-J model was shown to evaluate qualitatively the essential magnetic properties of a whole class of III-V materials[13]. Recently the model was also shown to successfully reproduce and explain quantitatively the measured optical conductivity in $\text{Ga}_{1-x}\text{Mn}_x\text{As}$ [15]. Here we calculate the T_{CS} , magnon density of states (DOS) (average and typical) along with the “mobility edge”, magnon spectral function and the spin stiffness as a function of the impurity concentration in optimally annealed $\text{Ga}_{1-x}\text{Mn}_x\text{As}$. The term optimally annealed implies that the concentration of compensating defects (As anti-sites or Mn interstitials) is negligible.

The one band V-J Hamiltonian describing the interaction between the carriers (holes or electrons) and the localized impurity spins is given by,

$$H = - \sum_{ij,\sigma} t_{ij} c_{i\sigma}^\dagger c_{j\sigma} + \sum_i J_i \mathbf{S}_i \cdot \mathbf{s}_i + \sum_{i\sigma} V_i c_{i\sigma}^\dagger c_{i\sigma} \quad (1)$$

where the hopping term $t_{ij}=t$ for i and j nearest neighbors, otherwise zero. $c_{i\sigma}^\dagger$ ($c_{i\sigma}$) is the creation (annihilation) operator of a hole of spin σ at site i . J_i is the p-d coupling (J_{pd}) between localized Mn spin \mathbf{S}_i ($|\mathbf{S}_i|=5/2$) and a spin carrier \mathbf{s}_i (p-band). The on-site potential V_i results from the substitution of Ga^{3+} by Mn^{2+} . Note that V_i is directly related to the position of the bound state with respect to the VB. $J_i=p_i J_{pd}$ and $V_i=p_i V$, where $p_i=1$ if the site is occupied by an impurity, otherwise zero. Note that x and p represent the Mn concentration and hole density respectively. The next task is to fix the model parameters. The bandwidth of GaAs host is of the order of $W\sim 7-8$ eV, hence we choose $t\approx 0.7$ eV (since our calculations are performed on a simple cubic lattice

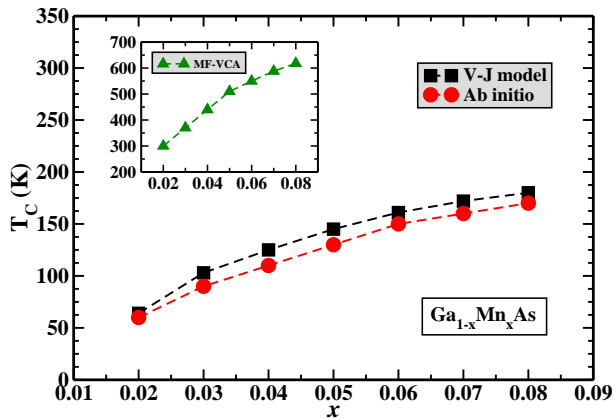


FIG. 1: (Color online) Curie temperature (in K) as a function of the Mn concentration (x). The squares represent our model and the circles correspond to ab-initio calculations. (Inset) The triangles correspond to the MF-VCA T_C (in K) as a function of x . (The size of the simple cubic lattice is $L=50$ and $N=50^3$ is the total number of sites.)

for which $W=12t$). $J_{pd}S$ is taken as 3 eV since the value of $J_{pd} \approx 1.2$ eV is already known for GaMnAs. The last parameter, the on-site potential V is the crucial one. It is set to 1.8t in order to reproduce the bound hybridized pd-states energy $E_b \approx 110$ meV with respect to the top of the VB. Now in the realistic material each Mn^{2+} provides one hole and $n_l=3$ degenerate p-d states near the top of the VB (here $p=x$ for the well annealed case). Thus for reasons of consistency our model calculations for optimally annealed samples are performed for the hole density $\bar{p}=p/n_l$. Then in both cases the IB is one-third filled (for more details see Ref.[15, 16]). Now we proceed to the calculation of the exchange couplings from our one band model. For a given impurity concentration ‘ x ’ and disorder configuration ‘ c ’, the Hamiltonian (1) is diagonalized exactly in both spin sectors. We have performed the calculations on simple cubic systems with sizes varying from $L=16$ to $L=24$ and the average over disorder is done for a few hundred configurations. A careful study of the finite size effect on the magnetic couplings has been made. The diagonalization provides us with the eigenvalues and eigenvectors denoted by $\{\omega_{\sigma,\alpha}^c, |\Psi_{\sigma,\alpha}^c\rangle\}$, where $\sigma=\uparrow, \downarrow$ and $\alpha=1,2,\dots,N$ ($N=L^3$ is the total number of sites), which are used to evaluate the couplings. The magnetic coupling between two localized spins is given by the generalized susceptibility[17]

$$\bar{J}_{ij}(x, \bar{p}) = -\frac{1}{4\pi S^2} \Im \int_{-\infty}^{E_F} Tr(\Sigma_i G_{ij}^{\uparrow}(\omega) \Sigma_j G_{ji}^{\downarrow}(\omega)) d\omega \quad (2)$$

where the Green’s functions are defined as $G_{ij}^{\sigma}(\omega) = \langle i\sigma | \frac{1}{\omega - \hat{H} + i\epsilon} | j\sigma \rangle$. It is found that the couplings calculated for well annealed $Ga_{1-x}Mn_xAs$ are rather short range and essentially ferromagnetic, and overall in good agreement with those from first principle studies[13, 18]. Now

the couplings that are used to calculate the T_C s and other magnetic properties are defined as $J_{ij}(x, p) = n_l \bar{J}_{ij}(x, \bar{p} = p/n_l)$, since we stress again that in our one band model each Mn^{2+} provides a single state unlike the 3 p-d states in the realistic case. Note that the same argument was used to calculate the transport properties, namely the optical conductivity, in $Ga_{1-x}Mn_xAs$ and excellent agreement with experimental results was obtained [15]. As we have found that the spin stiffness is sensitive to the size of the lattice on which the couplings are calculated, here the calculations have been performed systematically on considerably larger systems compared to previous studies[16] leading to an improvement in the couplings at large distances.

In Fig.1 we show the Curie temperature (in Kelvin) as a function of the Mn concentration for well annealed samples. To evaluate the Curie temperature, the effective dilute Heisenberg Hamiltonian $H_{Heis} = -\sum_{i,j} p_i p_j J_{i,j}(x, p) \mathbf{S}_i \cdot \mathbf{S}_j$, is treated within the SC-LRPA theory. After performing the Tyablikov decoupling and diagonalizing the above Hamiltonian we obtain the retarded Green’s functions given by

$$\mathcal{G}_{ij}^c(\omega) = \sum_{\alpha} \frac{2\langle S_j^z \rangle}{\omega - \omega_{\alpha}^c + i\epsilon} \langle i | \Phi_{\alpha}^c \rangle \langle \Phi_{\alpha}^c | j \rangle \quad (3)$$

where Φ_{α}^c and ω_{α}^c are now the eigenvalues and eigenvectors respectively of H_{Heis} for a given configuration ‘ c ’, and $\langle S_j^z \rangle$ is the local magnetization (for details see Ref.[8]). The diagonalization of the above Hamiltonian was performed on very large systems (typically $L=50$) together with a systematic average over a few hundred configurations of disorder. We have found that the T_C s shown here are comparable to those shown in Ref.[16]. As is clearly seen from the figure, our model calculations are in very good agreement with the T_C s obtained from first principle studies[7, 8, 19], which in turn reproduced accurately the experimental data[20–22]. We again stress the fact that there are no adjustable parameters in our model calculations. It is to be noted that this model can also be used to calculate the critical temperatures as well as the magnetic and transport properties for a whole class of DMS materials, which makes it all the more powerful[16]. Several attempts have been made to calculate the Curie temperature using mean field theories[23] but they have always resulted in overestimation. As an illustration the mean field Virtual Crystal Approximation (MF-VCA) T_C (inset of Fig.1) can be seen to already lead to room temperature for only 2% of Mn. Once again it shows the clear overestimation in the T_C values and hence the crucial importance of thermal fluctuations and dilution effects.

The average and typical magnon DOS as a function of the energy for different concentrations of Mn is plotted in Fig.2. The size of the simple cubic system in this case is $L=44$. The average magnon

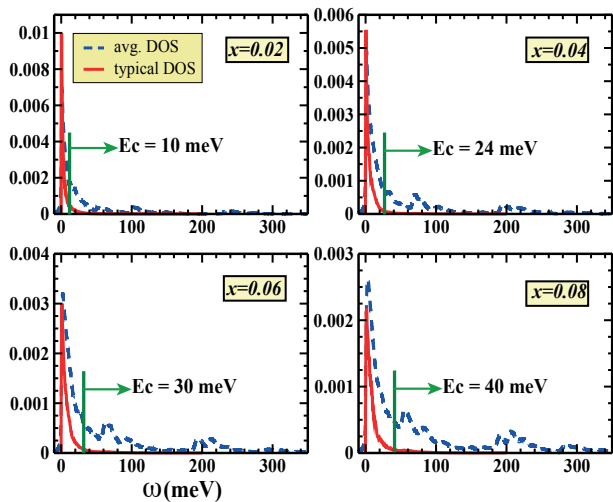


FIG. 2: (Color online) Magnon density of states (along the y axis) as a function of the energy ω (in meV) (along the x axis) for different Mn concentration x . The solid (dashed) line represents the typical (average) density of states.

DOS is given by $\rho_{avg}(\omega) = (1/N_{imp}) \sum_i \rho_i(\omega)$, where $\rho_i(\omega) = -(1/2\pi \langle S_i^z \rangle) \text{Im} \mathcal{G}_{ii}(\omega)$ is the local magnon DOS and N_{imp} is the total number of magnetic impurities (for details see Ref.[14]). As seen from the figure, the shape of $\rho_{avg}(\omega)$ exhibits a multipeak structure and changes significantly with increasing x . At sufficiently high dilution, close to the percolation, there is a drastic increase in the low energy DOS. This is due to formation of isolated impurity clusters at low concentrations which have their own zero-energy eigenmodes and these contribute to the average magnon DOS. However $\rho_{avg}(\omega)$ is not able to predict the nature of the magnon modes, whether they are extended or localized. For this we calculate the typical magnon DOS[24] which is given by $\rho_{typ}(\omega) = \exp(\langle \ln \rho_i(\omega) \rangle_c)$, where $\langle \dots \rangle_c$ denotes the average over disorder configurations. The typical magnon DOS is a local quantity and unlike $\rho_{avg}(\omega)$ it provides a direct access to the “mobility edge” separating the localized modes from the extended ones. The solid (red) line in the figure corresponds to $\rho_{typ}(\omega)$ and apparently there is no significant change in the overall shape with variation in dilution. We have evaluated from $\rho_{typ}(\omega)$ the energy E_c , which separates the localized from the extended states. The values are indicated in the figure. As we increase the Mn concentration E_c varies from 10 meV for $x=0.02$ to 40 meV for $x=0.08$. This shows that even for relatively larger concentrations most of the excitations consists of localized states (fractons)[25].

In the next figure, Fig.3, we show the magnon spectral function $A(\mathbf{q}, \omega) = -(1/\pi \langle \langle S^z \rangle \rangle) \text{Im} \mathcal{G}(\mathbf{q}, \omega)$, in the (\mathbf{q}, ω) plane over the entire Brillouin zone corresponding to three different concentrations of Mn. The spectral function is directly accessible by inelastic neutron scattering experiments and provides direct insight into the magnetic

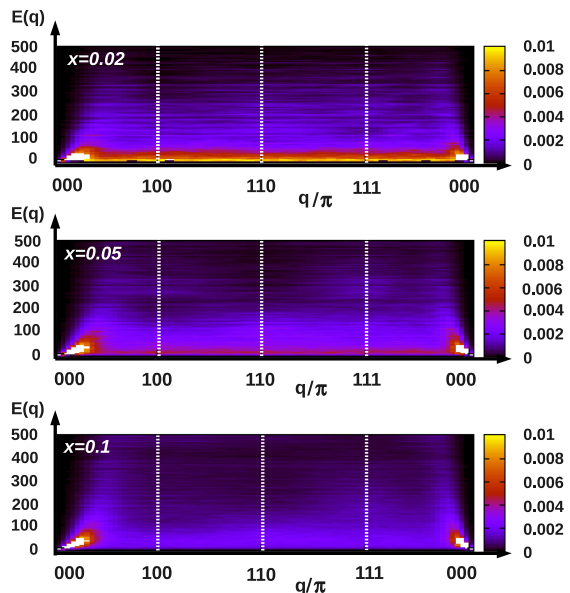


FIG. 3: (Color online) Spectral function $A(\mathbf{q}, \omega)$ in the (\mathbf{q}, ω) plane for different Mn concentration (x). The energy axis (y axis) is in meV. (The size of the simple cubic lattice is $L=44$).

excitation spectrum (details can be found in Ref.[14]). The average was done over a few hundred configurations of disorder but we found that increasing the number of configurations beyond 50 left the results almost unaffected. Now similar results were obtained for the excitation spectrum of $\text{Ga}_{1-x}\text{Mn}_x\text{As}$ [26] but it is to be noted the couplings in that case were calculated from first principle Tight Binding Linear Muffin Tin Orbital approach. We observe that well defined excitations exist only in a restricted region of the Brillouin zone essentially around the Γ point [$\mathbf{q}=(000)$]. The spectrum shows a significant broadening as we move away from the Γ point. This is in agreement with the typical DOS calculations shown in the previous figure. Thus we can see that our results are in very good agreement with those obtained from first principle studies cited above.

Now we proceed to calculate the spin stiffness as a function of the concentration of Mn. As a first step the magnon energy $\omega(\mathbf{q})$ is plotted as a function of \mathbf{q}^2 for different x , as shown in Fig.4. Here the $\omega(\mathbf{q})$ is extracted from the first peak of $A(\mathbf{q}, \omega)$ in the (100) direction. The system size varies from $L=32$ to $L=44$. The slope of these curves gives the spin stiffness $D(x)$ for various x . It is to be noted that the perfect linear nature of the dispersion curves justifies our claim that the average over disorder configurations is sufficient. In Fig.5 we have plotted the spin stiffness $D(x)$ as a function of x . We have found that $D(x)$ is sensitive to the couplings at large distances. These couplings appear to be strongly finite size dependent. Thus the calculation of $D(x)$ is performed using the couplings from different system sizes ranging from $L=16$

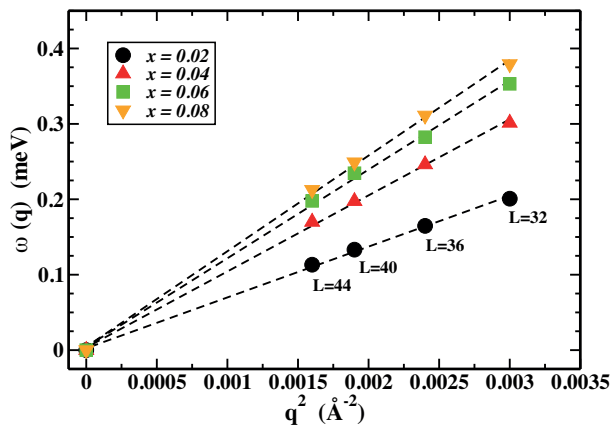


FIG. 4: (Color online) Magnon energy $\omega(\mathbf{q})$ (in meV) as a function of q^2 (in \AA^{-2}) for different concentration of Mn (x). (L is the size of the simple cubic lattice).

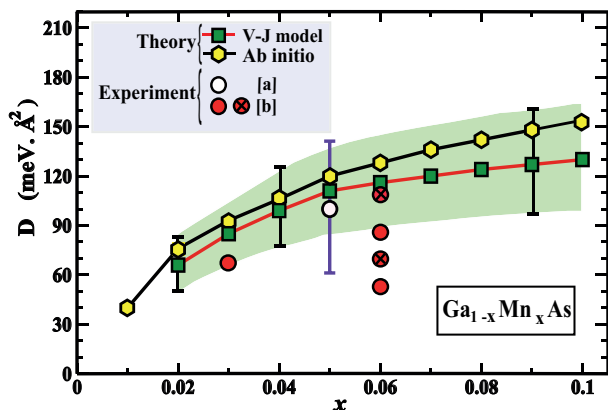


FIG. 5: (Color online) Spin stiffness D (in $\text{meV}\cdot\text{\AA}^2$) as a function of the Mn concentration (x). Squares correspond to our model, hexagons to ab-initio values[26] and circles [a,b] to experimental values from Ref.[28, 29]. (Note the circles with the cross denote the annealed samples from Ref.[29]).

to $L=24$, leading to error bars for $D(x)$ shown by the shaded region in the figure. It is to be noted that these couplings did not have a significant effect on the T_{CS} . In the figure we have shown the values of $D(x)$ obtained from ab-initio studies[26]. Note that the stiffness values shown in Fig.4 of Ref.[26] actually correspond to DS where $S=5/2$ [27]. Available experimental data for well annealed and as-grown samples[28, 29] are also shown in the figure. Surprisingly we find that the spin stiffness values from our model are in very good agreement, for the overall range of Mn concentration, with those obtained from first principle studies. We also note that the agreement with the experimental results of Sperl *et al.*[29] is for the well annealed sample of thickness 200nm. This is consistent with the fact that our couplings are calculated for optimally annealed samples. In Ref. [28] the authors have reported a value of $D \approx 100 \text{ meV}\cdot\text{\AA}^2$ measured by ferromagnetic resonance in as-grown sample for $x=0.05$,

which is also in good agreement with our results but then the error bar is about 40% and in all likelihood this stiffness should increase if the sample is optimally annealed. The deviation between our results and some experimental data could be explained by the fact that our calculations are performed for optimally annealed samples.

Thus to conclude, we have provided a quantitative model study of the magnetic excitations in Mn doped GaAs. The model parameters were fixed from the first principle calculations. We have calculated the magnon DOS, the “mobility edge” separating the localized states from extended ones, the dynamical spectral function, the spin stiffness and the T_{CS} as a function of the Mn concentration. We found a remarkable agreement between our theory and first principle studies for both the spin stiffness as well as the T_{CS} . At the same time we were able to reproduce most of the available experimental results. The strength of the model lies in the fact that it can be applied to a whole family of DMS materials and this proves to be the link between model approaches and first principle calculations.

One of us, AC, wishes to thank the RTRA Nanosciences Fondation for financial support.

-
- [1] K. Sato et al., Rev. Mod. Phys. **82**, 1633 (2010).
 - [2] T. Jungwirth et al., Rev. Mod. Phys. **78**, 809 (2006).
 - [3] T. Dietl et al., Science **287**, 1019 (2000).
 - [4] J. Inoue, S. Nonoyama and H. Itoh, Phys. Rev. Lett. **85**, 4610 (2000).
 - [5] J. Schliemann, J. König, H.H. Lin and A. H. MacDonald, Appl. Phys. Lett. **78**, 1550 (2001); J. König, T. Jungwirth and A. H. MacDonald, Phys. Rev. B **64**, 184423 (2001).
 - [6] G. Bouzerar, T. Ziman and J. Kudrnovský, Appl. Phys. Lett. **85**, 4941 (2004).
 - [7] L. Bergqvist et al., Phys. Rev. Lett. **93**, 137202 (2004).
 - [8] G. Bouzerar, T. Ziman and J. Kudrnovský, Europhys. Lett. **69**, 812 (2005).
 - [9] L. Bergqvist et al., Phys. Rev. B **67**, 205201 (2003).
 - [10] L. M. Sandratskii, P. Bruno and J. Kudrnovský, Phys. Rev. B **69**, 195203 (2004).
 - [11] K. S. Burch et al., Phys. Rev. Lett. **97**, 087208 (2006).
 - [12] R. Bouzerar, G. Bouzerar and T. Ziman, Phys. Rev. B **73**, 024411 (2006).
 - [13] R. Bouzerar, G. Bouzerar and T. Ziman, Europhys. Lett. **78**, 67003 (2007).
 - [14] A. Chakraborty and G. Bouzerar, Phys. Rev. B **81**, 172406 (2010).
 - [15] G. Bouzerar and R. Bouzerar, arXiv:1004.4446 (submitted).
 - [16] R. Bouzerar and G. Bouzerar, to appear in Europhys. Lett.
 - [17] M.I. Katsnelson and A. I. Lichtenstein, Phys. Rev. B **61**, 8906 (2000).
 - [18] J. Kudrnovský et al., Phys. Rev. B **69**, 115208 (2004).
 - [19] K. Sato, W. Schweika, P. H. Dederichs and H. Katayama-Yoshida, Phys. Rev. B **70**, 201202 (2004).

- [20] K. W. Edmonds et al., Appl. Phys. Lett. **81**, 3010 (2002); Phys. Rev. Lett. **92**, 037201 (2004).
- [21] F. Matsukura, H. Ohno, A. Shen and Y. Sugawara, Phys. Rev. B **57**, R2037 (1998).
- [22] D. Chiba, K. Takamura, F. Matsukura and H. Ohno, Appl. Phys. Lett. **82**, 3020 (2003).
- [23] Yu-Jun Zhao, T. Shishidou and A. J. Freeman, Phys. Rev. Lett. **90**, 047204 (2003); L. M. Sandratskii and P. Bruno, Phys. Rev. B **66**, 134435 (2002); K. Sato, P. H. Dederichs and H. Katayama-Yoshida, Europhys. Lett. **61**, 403 (2003).
- [24] V. Dobrosavljević, A. A. Pastor and B. K. Nikolić, Europhys. Lett. **62**(1), 76, 2003.
- [25] R. Orbach and K. W. Yu, J. Appl. Phys. **61**, 3689 (1987); A. Aharony, S. Alexander, O. Entin-Wohlman and R. Orbach, Phys. Rev. Lett. **58**, 132 (1987).
- [26] G. Bouzerar, Europhys. Lett. **79**, 57007 (2007).
- [27] G. Bouzerar, Erratum of [26] (submitted to Europhys. Lett.).
- [28] S. T. B. Goennenwein et al., Appl. Phys. Lett. **82**, 730 (2003).
- [29] M. Sperl et al., Phys. Rev. B **77**, 125212 (2008).